University of Tehran

Earth Observation and Geomatics Engineering

Online ISSN: 2588-4360

Homepage: https://eoge.ut.ac.ir/

An Integrated PolSAR and PolInSAR Framework for Landslide Detection Using Sentinel-1 Dual-Polarization SAR Data

Fatemeh Beigi[1], **Tayebe Managhebi**[✉], and **Mehdi Akhoondzadeh**[3]

1. School of Surveying and Geospatial Engineering, College of Engineering, University of Tehran, Tehran, Iran. E-mail: Fatemeh.beigi@ut.ac.ir
2. Corresponding author, Assistant Professor, Department of Photogrammetry and Remote Sensing, School of Surveying and Geospatial Engineering, College of Engineering, University of Tehran, Tehran, Iran. E-mail: t.managhebi@ut.ac.ir
3. Associate Professor, Department of Photogrammetry and Remote Sensing, School of Surveying and Geospatial Engineering, College of Engineering, University of Tehran, Tehran, Iran. E-mail: makhonz@ut.ac.ir

Article Info

Article type:

Research Article

Article history:

Received 2026-05-10

Received in revised form 2026-06-03

Accepted 2026-06-07

Available online 2026-07-24

Keywords:

LandSlide;
Machine Learning;
SAR Polarimetry;
SAR Polarimetric Interferometry;
Sentinel-1.

ABSTRACT

Rapid and reliable landslide detection in densely vegetated mountainous regions remains challenging, particularly under persistent cloud cover and adverse weather conditions where optical imagery becomes ineffective. This study proposes an integrated PolSAR and PolInSAR framework based on freely available Sentinel-1 dual-polarization SAR data for landslide detection following the 2024 Enga Province landslide event in Papua New Guinea. Polarimetric features, including entropy, alpha angle, radar vegetation index, cross-polarization ratio, and covariance matrix elements, were extracted to characterize changes in scattering mechanisms and vegetation structure. In addition, multi-temporal coherence features were generated from pre-event, post-event, and cross-event image pairs to capture decorrelation associated with surface displacement and structural changes. To evaluate the contribution of different feature groups, coherence-based, covariance-based, PolSAR, and integrated feature stacks were classified using machine learning approaches. Among the evaluated classifiers, random forest achieved the best overall performance with an overall accuracy of 0.88. Quantitative evaluation revealed that while the coherence-only and covariance-based stacks yielded accuracies of 0.63 and 0.82 respectively, the PolSAR feature stack provided strong discriminative capability with an accuracy of 0.87. The integration of polarimetric and interferometric features further improved classification performance, with the full feature stack achieving the highest accuracy (0.88) and F1-score of 0.88. These results demonstrate the robustness and effectiveness of utilizing dual-polarimetric Sentinel-1 data for rapid and accurate landslide mapping in complex, cloud-prone environments.

Cite this article: Beigi, F., Managhebi, T., & Akhoondzdeh, M. (2026). An Integrated PolSAR and PolInSAR Framework for Landslide Detection Using Sentinel-1 Dual-Polarization SAR Data. *Earth Observation and Geomatics Engineering*, Volume 10, Issue 1, Pages 93-104, http//doi.org/10.22059/eoge.2026.414122.1223

Publisher: University of Tehran.

DOI: https://orcid.org/10.22059/eoge.2026.414122.1223

1. Introduction

Landslides are among the most destructive natural hazards, causing significant loss of life and economic damage worldwide, particularly in mountainous regions with high rainfall. Timely and reliable identification of landslide-affected areas is therefore essential for effective disaster management, risk mitigation, and post event recovery planning. In this context, spaceborne remote sensing has become a key tool for monitoring and mapping landslides.

High-resolution optical satellite imagery, including data from WorldView-2, GeoEye-1, Sentinel-2, and PlanetScope, has been widely used for landslide detection. Recent studies have shown that the the integration of such data with machine learning and deep learning algorithms enables large-scale landslide mapping at regional and national levels (Amatya et al., 2019; Novellino et al., 2024). However, the applicability of optical imagery remains limited due to its dependence on weather conditions and solar illumination. Cloud cover, rainfall, and dense vegetation significantly restrict its effectiveness, particularly in tropical and mountainous environments.

To overcome these limitations, synthetic aperture radar (SAR) data have been increasingly utilized. SAR systems provide all-weather, day-and-night imaging capabilities, making them well suited for landslide monitoring. Multi-temporal interferometric SAR (MT-InSAR) techniques, such as PSInSAR and SBAS, are commonly applied to detect gradual surface deformation. Nevertheless, their performance degrades in densely vegetated areas due to temporal decorrelation and speckle noise, which also limits their ability to capture sudden landslide events (Ferretti et al., 2005; Higgins & Wdowinski, 2025; Pepe & Calò, 2017). In recent years, polarimetric SAR (PolSAR) and polarimetric interferometric SAR (PolInSAR) have attracted increasing attention as promising alternatives. Unlike conventional single-polarization SAR, which measures only backscattering intensity, PolSAR exploits polarization information to characterize different scattering mechanisms, such as surface, volume, and double-bounce scattering. This capability is particularly valuable in forested and mountainous terrains where conventional methods are limited. PolInSAR. By further combining polarimetric and interferometric information, PolInSAR enables more detailed characterization of surface structures and can reveal changes associated with landslides even under vegetation cover.

Several studies have explored the potential of PolSAR and PolInSAR data for landslide detection. For instance, Shibayama and Yamaguchi (2014), reported an increase in surface scattering and a decrease in volume scattering in landslide areas using ALOS-PALSAR data (Shibayama & Yamaguchi, 2014). Similarly, Lou et al. (2015), combining Claude-Pottier and Freeman-Durden decompositions on Radarsat-2 data, identified recent landslides. While these approaches highlight the sensitivity of polarimetric features to surface changes, they often suffer from high false alarm rates and limited consideration of topographic effects (Luo et al., 2015).

To improve detection performance, recent efforts have focused on multi-source data fusion. For example, Plank et al. (2016) combined pre-event optical imagery with post-event PolSAR data to enable rapid landslide mapping in vegetated regions. (Plank et al., 2016). Ohki et al. (2020), further integrated PolSAR, InSAR, and DEM data and showed that a random forest model achieved improved accuracy in complex mountainous environments (Ohki et al., 2020). Although these approaches enhance detection performance, their reliance on optical data or fully polarimetric SAR limits their operational feasibility.

Another line of researches has investigated the use of machine learning algorithms and multi-temporal change detection. Niu et al. (2021), for example, combined Wishart -based change detection with analytic hierarchy process to reduce false alarms in heterogeneous landscapes (Niu et al., 2021). While such methods are capable of capturing complex patterns, they generally require extensive training data and additional post-processing steps.

An important practical question concerns the level of polarimetric information required for reliable landslide detection. Comparative studies have shown that while quad-polarimetric data provide the highest accuracy, dual-polarimetric data can achieve comparable performance with significantly lower cost and wider availability (Park & Lee, 2019). This finding highlights the potential of freely available datasets such as Sentinel-1 for operational applications. More recently, Liu et al. (2025), demonstrated that multi-temporal PolInSAR approaches can improve coherence and reduce phase noise, particularly in densely vegetated areas (Liu et al., 2025).

In parallel with these polarimetric developments, recent advancements in landslide mapping have increasingly relied on deep learning (DL) techniques, particularly for handling complex spatial and temporal patterns in Earth observation datasets. Various convolutional neural network (CNN) architectures, such as U-Net and advanced multi-scale feature fusion networks, have been successfully applied to landslide segmentation tasks (Ghorbanzadeh et al., 2022; Jin et al., 2024; Orynbaikyzy et al., 2025). Furthermore, given the frequent limitations of optical sensors caused by adverse weather conditions during rainfall-triggered landslides, the application of SAR data has gained critical importance. Recent studies emphasize the necessity of utilizing SAR features, such as backscatter amplitude and multi-temporal characteristics, as well as integrating SAR with optical imagery to enhance automated landslide detection frameworks under challenging environmental conditions (Fu et al., 2024; Lindsay et al., 2025; Nava et al., 2022).

Despite significant progress, several fundamental research gaps remain. First, most studies have used full-polarimetric L-band data, which are limited in terms of temporal frequency and spatial coverage. In contrast, the potential of widely available Sentinel-1 dual-polarimetric data has not been fully explored within integrated PolInSAR frameworks. Second, the selection of informative PolSAR and PolInSAR features is often not systematically addressed, with many studies relying on predefined feature sets. Finally, the dependence on high-resolution and costly datasets restricts the scalability of existing approaches. To address these limitations, this study proposes an integrated PolSAR–PolInSAR framework for landslide detection in densely vegetated mountainous regions using Sentinel-1 dual-polarization SAR data. The main contributions of this study are summarized as follows:

• Development of an integrated PolSAR–PolInSAR framework based on freely available Sentinel-1 dual-polarization SAR data for landslide detection in densely vegetated regions.

• Extraction and joint analysis of coherence-based, covariance-based, and polarimetric decomposition features to characterize landslide-induced surface changes.

• Comparative evaluation of different feature stacks to investigate the relative contribution of PolSAR and PolInSAR information to landslide detection performance.

• Development of a cost-effective and operationally scalable framework suitable for rapid landslide mapping under cloudy and mountainous conditions.

2. Study Area and Data

This section introduces the study area and the datasets used in this research. It includes a description of the geographic and environmental characteristics of the selected region, followed by details of the SAR data and auxiliary datasets. Finally, the reference data used for training and validation are presented.

2.1. Study Area

The study focuses on Enga Province, located in the northern highlands of Papua New Guinea (approximately 5°25′S, 143°30′E) as shown in Figure 1.

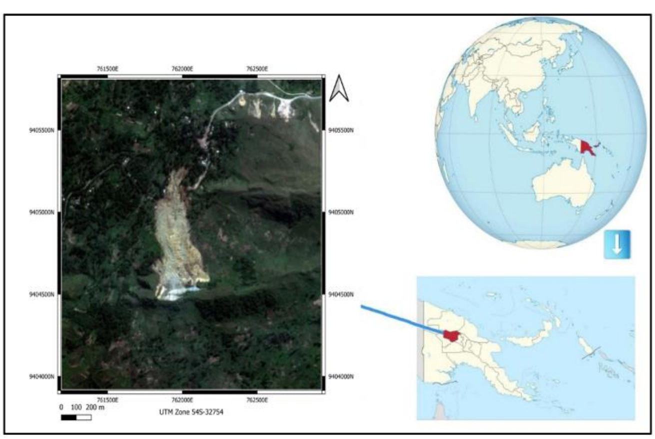

Figure 1. Location of the study area in Enga Province, Papua New Guinea.

This region is characterized by steep mountainous terrain, with elevations exceeding 3200 m, dense tropical forest cover, and a humid climate with intense and frequent rainfall (Hugh, 2012; MapLogs). These conditions, together with highly weathered geological formations, create an environment that is particularly prone to landslides (Robbins, 2014).

On 24 May 2024, a major landslide event occurred in this province, causing widespread destruction of villages, significant loss of life, and severe damage to infrastructure, while also blocking several waterways (IOM, 2024). An example of the affected area, captured by Sentinel-2 imagery shortly after the event, is presented in Figure 2.

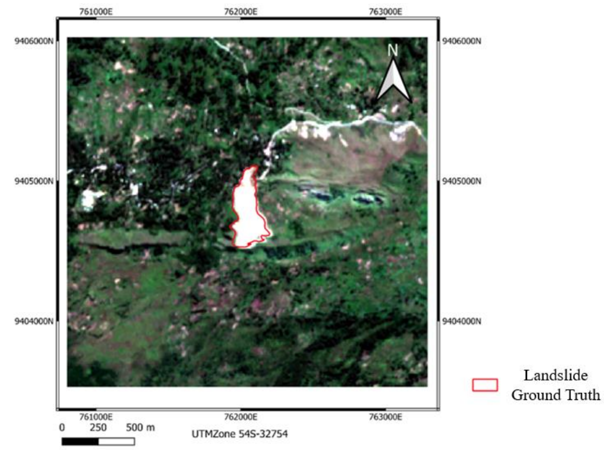

Figure 2. Sentinel-2 optical image of the landslide-affected area after the event

From a remote sensing perspective, this region represents a challenging yet highly relevant test site. Dense vegetation, persistent cloud cover, and complex topography significantly limit the effectiveness of optical imagery, while also complicating conventional SAR-based approaches. For this reason, the area provides a suitable benchmark for evaluating the capability of PolSAR and PolInSAR methods in detecting landslides under difficult environmental conditions.

2.2. Sentinel-1 SAR Data

Sentinel-1A C-band SAR imagery was used in this study, acquired in interferometric wide (IW) swath mode with dual polarization (VV and VH). The Sentinel-1 mission was selected due to its free and open data access, regular 12-day revisit cycle, and reliable all-weather imaging capability, making it particularly suitable for rapid disaster monitoring.

All images were acquired from a descending orbit to maintain geometric consistency throughout the time series. A total of four single look complex (SLC) images were used, including two pre-event acquisitions (6 May 2024 and 18 May 2024) and two post-event acquisitions (11 June 2024 and 23 June 2024). A minimal spatial baseline was also selected to reduce geometric decorrelation and improve coherence quality.

2.3. Auxiliary Data

The Copernicus digital elevation model (DEM) with a spatial resolution of 30 m was used to support SAR data processing. Specifically, it was applied for geometric terrain correction, and topographic normalization.

2.4. Ground Truth Data

Reference landslide polygons were obtained from United Nations Satellite Centre (UNOSAT), which generated the landslide inventory through visual interpretation of high-resolution GeoEye imagery (spatial resolution < 1 m) acquired shortly after the event. These datasets are widely considered reliable for post-disaster geomorphic assessments (UNOSAT, 2024).

3. Methodology

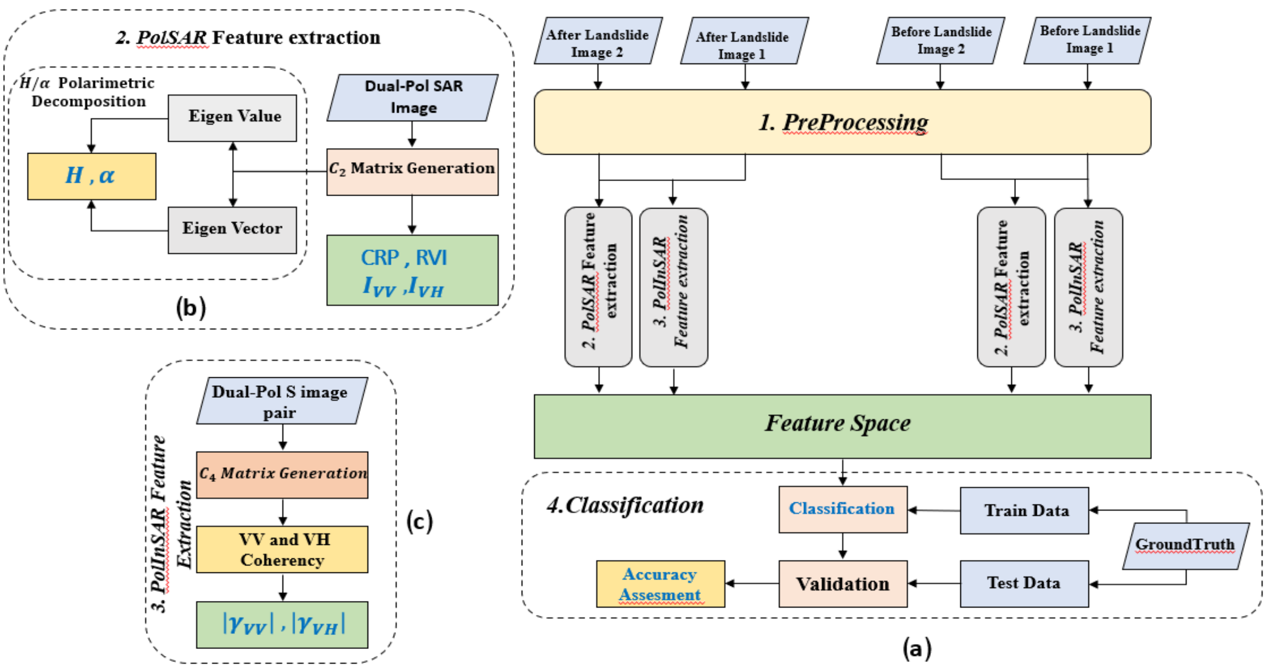

Figure 3. The proposed landslide detection framework using Sentinel-1 dual-pol data. (a) Overall workflow: from preprocessing and independent feature extraction to machine learning classification. (b) PolSAR feature extraction: deriving intensities, indices (RVI, CRP), and H/α decomposition parameters from the C2 covariance matrix. (c) PolInSAR feature extraction: computing polarimetric coherence magnitudes from the covariance matrix.

This section describes the implementation of the proposed landslide detection framework, including pre-processing, feature extraction, and classification stages. As illustrated in Figure 3, the proposed workflow consists of four main components: (1) pre-processing of Sentinel-1 SAR data and reference samples, (2) extraction of polarimetric features from dual-polarization SAR observations, (3) generation of PolInSAR coherence features from multi-temporal image pairs, and (4) machine learning-based classification and evaluation.

3.1. Fundamental Concepts

This subsection introduces the theoretical background of the features used in this study. Two main groups of features are considered: polarimetric features derived from scattering characteristics, and polarimetric interferometric features derived from coherence analysis. These features are designed to capture both structural and temporal changes associated with landslide events.

3.1.1. Polarimetric Feature

Polarimetric SAR observations provide information about the interaction between the electromagnetic wave and the Earth's surface, which depends on the geometric and dielectric properties of the target. This interaction can be described using the scattering vector and its statistical representations.

For dual-polarization SAR data, the scattering behavior is commonly represented by the scattering vector in the lexicographic basis as (Lee & Pottier, 2009),

$$L = [S_{HH} \ \sqrt{2}S_{HV} \ S_{VV}]^{t}$$

where S_{VV} and S_{VH} represent the complex backscattering coefficients for co-polarized (vertical transmit–vertical receive) and cross-polarized (vertical transmit–horizontal receive) channels, respectively. These coefficients contain both amplitude and phase information and reflect the scattering behavior of the target. Based on the scattering vector, the second-order statistical properties of the scattering process can be described using the covariance matrix C_2, defined as (Lee & Pottier, 2009),

$$\mathbf{C}_2 = \begin{bmatrix} \langle |S_{VV}|^2 \rangle & \langle S_{VV} S_{VH}^* \rangle \\ \langle S_{VH} S_{VV}^* \rangle & \langle |S_{VH}|^2 \rangle \end{bmatrix} \tag{2}$$

where $\langle \bullet \rangle$ denotes ensemble averaging and $*$ represents the complex conjugate. The diagonal elements of this matrix correspond to the backscatter intensities of the co-polarized and cross-polarized channels, while the off-diagonal elements contain information about the correlation between them.

The elements of the covariance matrix can be used for two main purposes. First, they enable the derivation of polarimetric indices related to vegetation structure and surface roughness. Second, they provide the basis for polarimetric decomposition techniques, which aim to identify dominant scattering mechanisms. Among the indices derived directly from the covariance matrix, the cross-polarization ratio (CPR) is defined as (Tolometti et al., 2022),

$$\mathrm{CPR} = \frac{\langle |S_{VH}|^2 \rangle}{\langle |S_{VV}|^2 \rangle} \tag{3}$$

CPR quantifies the relative contribution of cross-polarized scattering and is sensitive to surface roughness and structural heterogeneity. Higher CPR values typically indicate irregular surfaces or complex vegetation structures (Lindsay et al., 2025).

The radar vegetation index (RVI) is another important parameter, defined as (Kim et al., 2012),

$$\mathrm{RVI} = \frac{4\langle |S_{VH}|^2 \rangle}{\langle |S_{VV}|^2 \rangle + \langle |S_{VH}|^2 \rangle} \tag{4}$$

RVI is widely used as an indicator of vegetation density and volume scattering. High values are generally associated with dense vegetation, while lower values indicate sparse vegetation or exposed surfaces.

In addition to these indices, polarimetric decomposition techniques can be applied to extract physically interpretable features. For dual-polarization data, the H/α decomposition remains a suitable and widely used approach, as it provides a simplified yet meaningful representation of scattering behaviour based on the available information. This decomposition is based on the eigenvalue analysis of the covariance matrix. Entropy (H) is defined as (Lee & Pottier, 2009),

$$H = -\sum_{i=1}^{n} p_i \log_n(p_i) \tag{5}$$

where p_i is the probability of each scattering mechanism and can be defined based on the eigenvalues of the covariance matrix as,

$$p_i = \frac{\lambda_i}{\sum \lambda_i} \tag{6}$$

where λ denotes the eigenvalue. Entropy measures the randomness of the scattering process. Low values indicate a dominant and deterministic scattering mechanism, such as surface scattering, while high values correspond to complex and random scattering, typically associated with volumetric targets like vegetation.

The alpha angle, which describes the dominant scattering mechanism, is defined as,

$$\alpha = \sum_{i=1}^{n} p_i \alpha_i \tag{7}$$

where α_i is obtained from the eigenvector associated with each eigenvalue. Lower values of alpha are associated with surface scattering from relatively smooth surfaces, whereas higher values indicate volume scattering from randomly oriented structures.

From a physical perspective, landslide events often result in the removal of vegetation and exposure of bare soil. This leads to a transition from volume-dominated scattering to surface-dominated scattering, which is typically reflected in decreased entropy and alpha values, along with changes in CPR and RVI (Yonezawa et al., 2012).

3.1.2. Polarimetric Interferometric Feature

While polarimetric features describe the scattering behavior of the surface, interferometric SAR (InSAR) provides information about phase differences between acquisitions, which are sensitive to surface deformation. However, conventional InSAR techniques are often limited in vegetated areas due to temporal decorrelation and volume scattering effects. On the other hand, PolSAR captures scattering mechanisms but lacks temporal sensitivity to structural changes.

Polarimetric interferometric SAR (PolInSAR) combines these two approaches by exploiting both polarimetric and interferometric information. In particular, it enables the analysis of coherence in different polarization bases, providing enhanced sensitivity to structural and temporal changes in complex environments such as forested areas.

In the PolInSAR framework, the statistical properties of two SAR acquisitions are jointly described by the covariance matrix C4, which is constructed from the lexicographic scattering vectors of the image pair. This matrix can be expressed as,

$$C_4 = \langle LL^{\dagger} \rangle = \begin{bmatrix} \langle L_1 L_1^{\dagger} \rangle & \langle L_1 L_2^{\dagger} \rangle \\ \langle L_2 L_1^{\dagger} \rangle & \langle L_2 L_2^{\dagger} \rangle \end{bmatrix} \quad (8)$$

where C4 contains the cross-correlation terms of the scattering coefficients from both acquisitions. The elements of this matrix provide the necessary components for coherence estimation. In this framework, the complex coherence between two arbitrary polarization channels S1 and S2 is defined as (Tamm et al., 2016),

$$\gamma = |\gamma| e^{i\phi} = \frac{\langle S_1 S_2^* \rangle}{\sqrt{\langle S_1 S_1^* \rangle \langle S_2 S_2^* \rangle}} \quad (9)$$

where subscripts 1 and 2 denote two temporal acquisitions, $|\gamma|$ is the coherence magnitude which reflects the degree of similarity between two signals, and ϕ denotes the coherence phase corresponds to the interferometric phase. The magnitude of coherence ranges from 0 to 1. High coherence values indicate stable scattering behavior between acquisitions, whereas low values correspond to decorrelation caused by changes in the observed scene. Several factors contribute to coherence loss, including temporal decorrelation due to surface changes, volume decorrelation in vegetated areas, geometric decorrelation, and system noise.

In the context of landslides, surface displacement, vegetation removal, and structural disturbance lead to significant changes between pre-event and post-event acquisitions. These changes typically result in a noticeable reduction in coherence, particularly in cross-event image pairs. Therefore, coherence can serve as an effective indicator for detecting landslide-affected areas, especially in regions with dense vegetation where conventional methods face limitations.

3.2. Proposed Method

This section describes the implementation of the proposed framework, including pre-processing, feature extraction, and classification.

3.2.1. Pre-processing

Pre-processing was carried out separately for polarimetric and interferometric analyses, as each requires specific preparation steps.

For polarimetric feature extraction, Sentinel-1 IW SLC data were first processed to ensure spatial continuity and suitability for polarimetric analysis. Due to the TOPSAR acquisition mode, each scene consists of multiple bursts acquired sequentially along the azimuth direction, which inherently exhibit slight overlaps and discontinuities at burst boundaries. To address this, a deburst operation was applied to merge the bursts into a continuous image, eliminating phase and geometric discontinuities and enabling consistent pixel-wise analysis.

Following this, polarimetric covariance matrices were generated from the VV and VH channels, forming the basis for subsequent feature extraction. To reduce speckle noise while preserving structural and polarimetric information, a refined Lee filter with a 5×5 window was applied. This filtering step ensures a balance between noise suppression and the preservation of physical features, particularly in heterogeneous areas.

Finally, terrain correction was performed using the Copernicus DEM with 30 m spatial resolution. The Range-Doppler approach was employed to correct geometric distortions caused by topography and to geocode the data into the UTM Zone 54S coordinate system. All datasets were resampled to a spatial resolution of 10 m using bilinear interpolation to maintain spatial consistency.

For interferometric processing, precise co-registration of image pairs was performed using the back-geocoding approach, where the slave image was aligned to the master image based on geometric information and the Copernicus DEM. This step ensures sub-pixel alignment, which is essential for reliable coherence estimation. To further refine the alignment, the enhanced spectral diversity (ESD) technique was applied to correct residual geometric errors and improve co-registration accuracy.

In addition, the reference landslide polygons obtained from the UNOSAT inventory were reprojected to UTM Zone 54S (EPSG:32754) and resampled to a spatial resolution of 10 m to ensure spatial consistency with the SAR-derived feature layers. The processed reference data were subsequently used for supervised training and quantitative accuracy assessment of the proposed landslide detection framework.

3.2.2. PolSAR Feature Extraction

Polarimetric features were derived from the dual-polarization covariance matrix constructed from VV and VH channels, as described in Section 3.1.

Entropy (H) and alpha angle (α) were obtained through eigenvalue decomposition to characterize scattering randomness and dominant scattering mechanisms, respectively. Landslide-affected areas exhibited noticeable reductions in both H and α, indicating a transition from volume scattering (vegetated surfaces) to surface scattering (exposed soil and debris).

In addition, the radar vegetation index (RVI) and cross-polarization ratio (CPR) were computed to quantify vegetation density and depolarization effects. Both indices showed reduced values in landslide areas, consistent with vegetation removal and changes in surface roughness.

Furthermore, covariance matrix elements were extracted separately for pre-event and post-event acquisitions to capture temporal variations in surface properties such as moisture, roughness, and structural conditions.

3.2.3. PolInSAR Feature Extraction

Following the pre-processing stage, coherence was estimated from co-registered Sentinel-1 image pairs to capture temporal and structural changes associated with landslide events. Two pre-event and two post-event acquisitions were available, enabling the generation of coherence features across multiple temporal configurations.

Coherence was computed for both VV and VH polarization channels using three image pair combinations, including pre-event pairs, post-event pairs, and cross-event (pre–post) pairs. The computation was performed based on Equation (6), using a 5×5 averaging window to ensure a balance between noise reduction and spatial detail preservation. This process resulted in a total of six coherence features.

Subsequently, the coherence maps were geocoded and terrain-corrected using the Copernicus DEM with a spatial resolution of 30 m. All datasets were projected to the UTM Zone 54S coordinate system (EPSG:32754) and resampled to a ground resolution of 10 m using bilinear interpolation, ensuring spatial consistency with other feature layers.

The resulting georeferenced coherence maps provide valuable information on surface stability. In particular, areas affected by landslides exhibit significant coherence loss due to surface displacement, vegetation removal, and structural disruption. Therefore, these coherence features serve as effective PolInSAR inputs for distinguishing unstable and landslide-affected areas in the classification process.

3.2.4. Classification

To evaluate the contribution of different feature types, four feature stacks were constructed:

- coherence-only stack (six coherence features)
- polarimetric-only stack (H, α, RVI, CPR)
- covariance-based stack (VV and VH intensities from pre- and post-event acquisitions)
- full stack (all features combined)

These configurations enable a comparative analysis of the discriminative capability of coherence-based, polarimetric, and intensity-based information for landslide detection.

Three machine learning classifiers were evaluated using the full feature set, including SVM, RF, and XGBoost classifiers.

3.3. Accuracy Assessment

Classification performance was evaluated based on the confusion matrix using overall accuracy, kappa coefficient, F1-score, producer’s accuracy, and user’s accuracy. These metrics provide a comprehensive assessment of classification performance in terms of both overall agreement and class-specific accuracy.

To ensure statistical and spatial independence between samples and to reduce the effect of spatial autocorrelation, a spatially disjoint sampling strategy was adopted. A total of 100 landslide samples and 200 non-landslide samples were collected, while enforcing a minimum spatial distance constraint of 20 m for landslide samples and 50 m for non-landslide samples. In addition, a balanced random sampling approach was employed to mitigate class imbalance effects. The dataset was subsequently divided into 70% training samples and 30% testing samples for model development and evaluation.

4. Results

This section presents the experimental results of the proposed framework for landslide detection using PolSAR and PolInSAR features derived from Sentinel-1 data. First, the behavior of the extracted polarimetric and interferometric features before and after the landslide event is analyzed. Subsequently, the performance of different machine learning classifiers is evaluated, followed by a comparative assessment of the proposed feature stacks for landslide detection.

4.1. Feature Representation Analysis

To investigate the sensitivity of the extracted features to landslide-induced surface changes, the spatial behavior of polarimetric and interferometric features was analyzed before and after the event. The observed variations provide insight into changes in scattering mechanisms, vegetation structure, and surface stability within the landslide-affected areas.

To better understand the surface changes caused by the landslide event, the spatial variations of VV and VH backscatter intensities before and after the event were first examined. As shown in Figure 4, the landslide area is characterized by increased VV intensity and reduced VH intensity after the event. This pattern reflects a transition from vegetation-dominated volume scattering to surface-dominated scattering following slope failure. The increase in VV response is associated with the exposure of bare soil and debris surfaces, whereas the reduction in VH intensity indicates the loss of volumetric scattering caused by vegetation destruction. These observations demonstrate that covariance matrix elements are sensitive to landslide-induced changes in surface structure and vegetation cover.

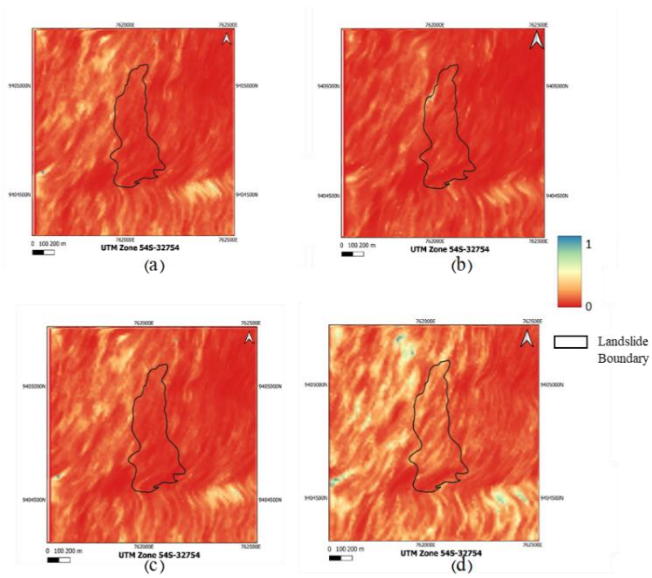

Figure 4. Backscatter intensity maps of VV and VH polarizations before and after the landslide event: (a) VV after, (b) VV before, (c) VH after, and (d) VH before

To further investigate changes in scattering mechanisms, the spatial distribution of the alpha parameter before and after the landslide event was analyzed. Figure 5 illustrates that α values substantially decreased within the landslide zone following the event. The alpha angle is directly related to the dominant scattering mechanism. Higher α values are generally associated with volumetric scattering originating from dense vegetation and heterogeneous three-dimensional structures, whereas lower values correspond to surface scattering from relatively smooth and homogeneous surfaces. The reduction of α within the landslide area indicates that the complex volumetric structure of the vegetation cover was disrupted after the event, exposing a simpler surface dominated by soil and debris. This behavior is physically consistent with the removal of vegetation and the increased contribution of surface scattering following slope failure.

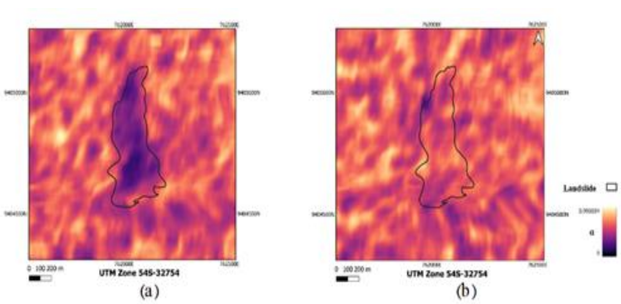

Figure 5. Alpha angle (α) maps: (a) after and (b) before the landslide event

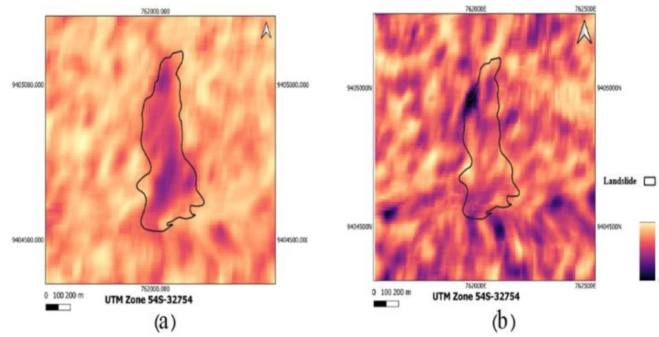

Figure 6. Entropy (H) maps: (a) after and (b) before the landslide event

A similar trend can also be observed in the entropy maps before and after the event.

Figure shows a significant decrease in entropy values within the landslide-affected region after the occurrence of the landslide.

Entropy represents the randomness and complexity of the scattering process and typically exhibits higher values in densely vegetated regions characterized by heterogeneous volumetric scattering. The observed reduction in entropy indicates that the complex scattering structure associated with vegetation cover was substantially weakened after the landslide. As vegetation was removed and the surface became more homogeneous, the scattering behavior shifted toward a more deterministic surface-scattering mechanism, resulting in lower entropy values.

To evaluate the temporal stability of the surface and the structural changes induced by the landslide, coherence magnitude maps were further analyzed for both VV and VH polarization channels. Figure presents the coherence maps derived from pre-event, post-event, and cross-event image pairs.

A significant reduction in coherence magnitude can be observed within the landslide area, particularly in the cross-event coherence maps. This coherence loss reflects both structural surface changes and the loss of phase consistency caused by the landslide event. Surface displacement, vegetation destruction, and changes in scattering mechanisms contribute to temporal decorrelation, making coherence an effective indicator of landslide activity.

Interestingly, comparison between pre-event and post-event coherence maps reveals localized coherence increases after the event, particularly in the VV channel. In densely vegetated regions, coherence is typically low due to temporal variations in vegetation structure and canopy orientation. Following the landslide, however, the removal of vegetation and exposure of bare surfaces increase geometric stability between acquisitions, resulting in higher coherence values. A similar trend can also be observed in the VH channel, confirming that the transition from forested terrain to exposed soil surfaces modifies the scattering behavior and improves temporal coherence after the event. These observations demonstrate the strong sensitivity of coherence features to landslide-induced surface changes.

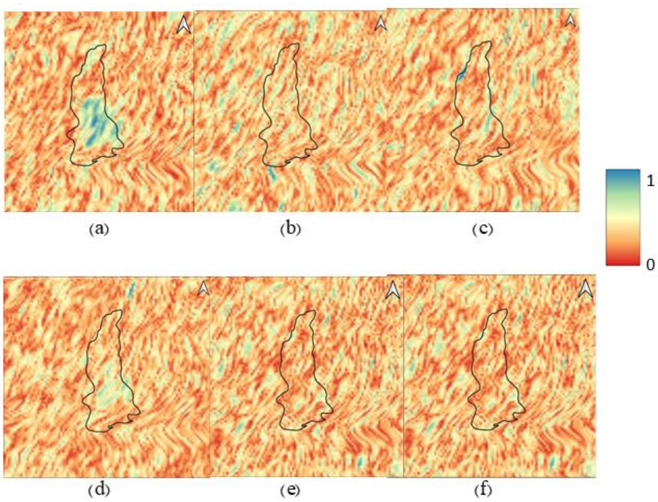

Figure 7. Coherence magnitude maps for VV (a–c) and VH (d–f) polarizations derived from post-event, cross-event, and pre-event image pairs, respectively

To further investigate vegetation-related changes caused by the landslide, the radar vegetation index (RVI) was analyzed before and after the event. As illustrated in Figure 6, the landslide area exhibits a noticeable reduction in RVI values following the event. Since RVI is strongly associated with volumetric scattering from vegetation canopies and heterogeneous forest structures, the observed decrease indicates substantial vegetation loss and weakening of volume scattering within the affected area. This behavior is consistent with the trends observed in other polarimetric features and further confirms the transition from vegetation-dominated scattering to surface-dominated scattering after the landslide event. These results suggest that RVI provides complementary information for characterizing landslide-induced changes in vegetation structure and surface conditions.

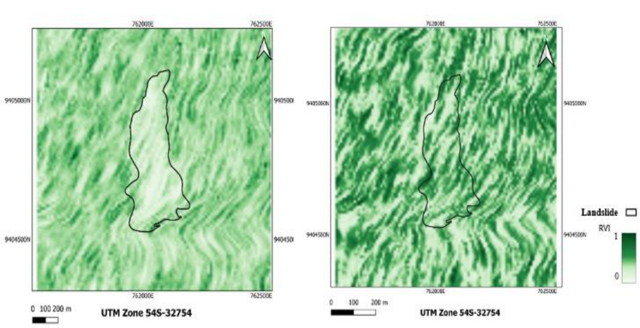

Figure 6. Radar vegetation index (RVI) maps: (a) after and (b) before the landslide event

Finally, the spatial variations of the cross-polarization ratio (CPR) before and after the landslide event were also examined. In contrast to other polarimetric features, CPR showed only limited differences within the landslide area after the event, as can be seen in Figure 7.

This relatively weak response suggests that CPR was less sensitive to the structural changes caused by the landslide in the study area. Although minor local variations can be observed, the overall spatial pattern remained relatively similar between pre-event and post-event conditions. This behavior may be related to the complex scattering environment of the forested terrain, where multiple scattering contributions reduce the separability of CPR responses. Nevertheless, CPR was retained as a complementary feature within the proposed framework, since its combined use with other polarimetric and interferometric features may still contribute to the overall classification performance.

In summary, the combination of covariance-based indices and decomposition-derived parameters provides complementary information about surface structure, vegetation condition, and dominant scattering behavior.

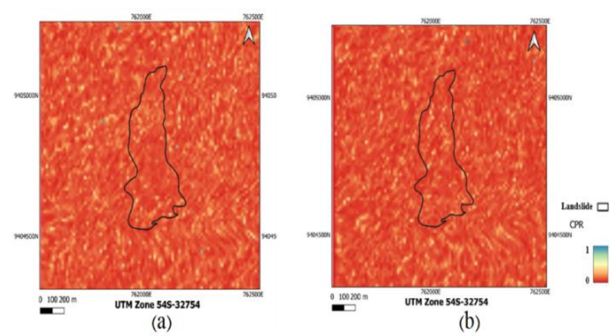

Figure 7. Cross-polarization ratio (CPR) maps: (a) after and (b) before the landslide event

4.2. Classifier Evaluation

To identify the most suitable classification algorithm for landslide detection, three widely used machine learning classifiers were evaluated using the full feature stack, including SVM, RF, and XGBoost classifiers.

For the RF model, 100 decision trees were employed using the Gini impurity criterion for node splitting, while bootstrap aggregation was enabled to improve model robustness. A minimum leaf size of one sample was considered, and the final classification threshold was selected by maximizing the F1-score on the training dataset.

The SVM classifier was implemented using a radial basis function (RBF) kernel to model the non-linear separability of landslide and non-landslide classes in the multidimensional feature space.

For the XGBoost classifier, the model was configured with 100 trees, a maximum tree depth of 4, and a learning rate of 0.1. These settings were selected to balance classification accuracy and generalization capability while reducing the risk of overfitting to noisy SAR-derived features. Table 1 presents the quantitative comparison of the classification results obtained from the three models.

Table 1. Performance comparison of classifiers using the full feature stack

Classifier	Accuracy	Precision	Recall	Kappa
RF	0.88	0.90	0.87	0.76
SVM	0.83	0.81	0.87	0.67
XGBoost	0.85	0.84	0.87	0.70

All three classifiers were able to distinguish landslide from non-landslide areas with relatively high accuracy. however, noticeable differences were observed in their overall performance.

Among the evaluated models, RF achieved the best results across all evaluation metrics, providing the most balanced precision and recall together with the lowest level of false positives. SVM achieved a recall comparable to RF but showed lower precision, indicating a higher number of false alarms. XGBoost exhibited intermediate performance, outperforming SVM in precision while still remaining less accurate and stable than RF. For the landslide class, all three classifiers achieved a recall of approximately 0.87, demonstrating strong capability in identifying landslide-affected areas. Nevertheless, the overall performance of RF indicates better generalization ability and classification robustness, making it the most suitable classifier for the subsequent feature stack analysis.

4.3. Land Slide Detection Results

After selecting random forest as the optimal classification algorithm, the performance of different feature stacks was further evaluated to investigate the contribution of coherence-based, polarimetric, and covariance-based features to landslide detection. Four feature configurations, including coherence-only, covariance-based, PolSAR, and full feature stacks, were independently classified using the RF model.

Table 2 summarizes the quantitative performance obtained from each feature stack.

Table 2. Classification performance of different feature stacks using the RF classifier.

Feature Stack	Accuracy	Precision	Recall	F1-score
Coherence stack	0.63	0.60	0.82	0.69
C-matrix stack	0.82	0.85	0.77	0.81
PolSAR stack	0.87	0.84	0.90	0.87
Full stack	0.88	0.90	0.87	0.88

The coherence-only stack achieved the weakest overall performance, with relatively low accuracy and precision despite maintaining acceptable recall values. This result indicates that coherence information alone is capable of identifying many landslide-affected areas but also introduces a considerable number of false positives. The reduced performance can be attributed to the sensitivity of coherence to multiple decorrelation sources, including vegetation dynamics, temporal changes, and geometric effects.

The covariance-based stack produced a substantial improvement in classification accuracy, demonstrating that intensity-related information extracted from VV and VH channels contains valuable information regarding surface and vegetation changes caused by the landslide event.

Among the individual feature groups, the PolSAR stack achieved the best performance, with the highest recall and a strong balance between precision and overall accuracy. These results confirm that polarimetric features such as entropy, alpha angle, RVI, and CPR effectively capture changes in scattering mechanisms associated with vegetation destruction and surface exposure following the landslide.

The full feature stack provided the highest overall accuracy and F1-score, indicating that the integration of coherence, covariance, and polarimetric features improves the robustness of landslide detection. Although the improvement compared to the PolSAR stack is relatively moderate, the combined feature space provides complementary information that enhances the separability between landslide and non-landslide areas.

Figure 8 illustrates the final landslide detection result obtained from the proposed framework using the optimal feature stack and the RF classifier. The produced probability map successfully delineates the main landslide body and demonstrates strong agreement with the reference landslide boundary. High probability values are concentrated within the central landslide region, while surrounding stable areas are generally associated with low probabilities. The spatial

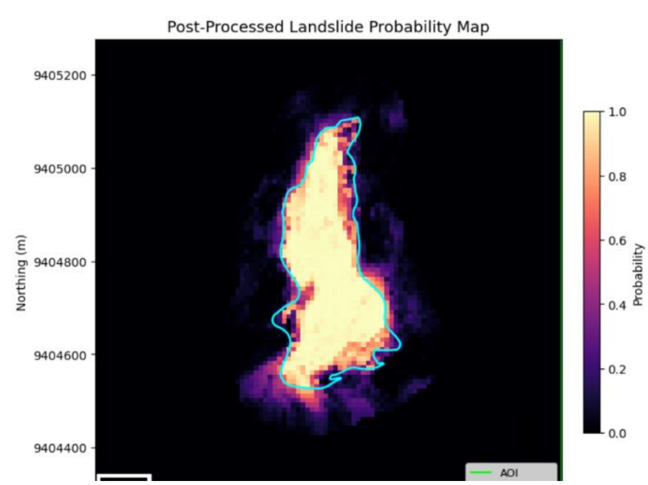

Figure 8. Final landslide probability map based on the integrated feature stack using RF classifier. The cyan boundary represents the reference landslide inventory, while warmer colors indicate higher landslide probability values.

distribution of the detected landslide area indicates that the integration of polarimetric and interferometric features effectively captures the structural and scattering changes caused by the landslide event. In particular, the transition from vegetated terrain to exposed soil and debris, together with the associated coherence variations, contributes to the clear separation between landslide and non-landslide regions. Although a limited number of low-probability responses can be observed around the landslide boundary, likely due to residual vegetation effects and transitional surface conditions, the overall classification result demonstrates high spatial consistency and reliable delineation capability in this densely vegetated mountainous environment.

5. Conclusion

This study presented a landslide detection framework based on the integration of PolSAR and PolInSAR features derived from freely available Sentinel-1 dual-polarization SAR data. The proposed approach exploited polarimetric decomposition parameters, covariance matrix elements, and multi-temporal coherence features to characterize landslide-induced changes in scattering behaviour, vegetation structure, and surface stability in a densely forested mountainous region of Papua New Guinea.

The feature analysis demonstrated that the landslide event caused a clear transition from volume-dominated scattering to surface-dominated scattering, reflected by decreases in entropy, alpha angle, VH intensity, RVI, and coherence magnitude, together with increased VV backscatter intensity. These variations confirm the sensitivity of both polarimetric and interferometric features to vegetation destruction and surface deformation caused by the landslide.

Among the evaluated machine learning classifiers, random forest achieved the best overall performance and was therefore selected for subsequent classification experiments. Comparative analysis of different feature stacks showed that the PolSAR feature set provided the strongest individual performance, while the integration of all features achieved the highest overall classification accuracy.

The obtained results indicate that freely available Sentinel-1 dual-polarization data can provide reliable and operationally applicable information for landslide detection in densely vegetated regions. The proposed framework demonstrates the potential of combining PolSAR and PolInSAR features for rapid landslide mapping, particularly in areas where optical imagery is limited by cloud cover and adverse weather conditions.

Although the proposed framework demonstrated promising performance in densely vegetated mountainous terrain, its generalization capability requires further investigation. Future research should evaluate the framework across multiple landslide events and geographically diverse study areas to assess its robustness under varying climatic, topographic, and vegetation conditions. Furthermore, integrating external topographic factors and advanced deep learning approaches could be explored to further improve detection accuracy and facilitate operational applicability at regional and global scales.

References

Amatya, P., Kirschbaum, D., & Stanley, T. (2019). Use of Very High-Resolution Optical Data for Landslide Mapping and Susceptibility Analysis along the Karnali Highway, Nepal. *Remote Sensing*, *11*(19), 2284. https://doi.org/https://doi.org/10.3390/rs11192284

Ferretti, A., Prati, C., Rocca, F., Casagli, N., Farina, P., & Young, B. (2005). Permanent Scatterers technology: a powerful state of the art tool for historic and future monitoring of landslides and other terrain instability phenomena. Proceedings of the International Conference on Landslide Risk Management, Vancouver, BC, Canada,

Fu, S., De Jong, S. M., Hou, X., de Vries, J., Deijns, A., & de Haas, T. (2024). A Landslide Dating Framework Using a Combination of Sentinel-1 SAR and Sentinel-2 Optical Imagery. *Engineering Geology*, *329*, 107388. https://doi.org/10.1016/j.enggeo.2023.107388

Ghorbanzadeh, O., Xu, Y., Ghamisi, P., Kopp, M., & Kreil, D. (2022). Landslide4Sense: Reference Benchmark Data and Deep Learning Models for Landslide Detection. *IEEE Transactions on geoscience and remote sensing*, *60*, 1–17. https://doi.org/10.1109/tgrs.2022.3215209

Higgins, M., & Wdowinski, S. (2025). InSAR Detection of Slow Ground Deformation: Taking Advantage of Sentinel-1 Time Series Length in Reducing Error Sources. *Remote Sensing*, *17*(14), 2420. https://doi.org/https://doi.org/10.3390/rs17142420

Hugh, L. D. (2012). The geology of New Guinea - the cordilleran margin of the Australian continent. *International Union of Geological Sciences*, *35*(1), 87–102. https://doi.org/10.18814/epiiugs/2012/v35i1/008

Jin, Y., Liu, X., & Huang, X. (2024). EMR-HRNet: A Multi-Scale Feature Fusion Network for Landslide Segmentation from Remote Sensing Images. *Sensors*, *24*(11), 3677. https://doi.org/10.3390/s24113677

Kim, Y., Jackson, T., Bindlish, R., Lee, H., & Hong, S. (2012). Radar Vegetation Index for Estimating the Vegetation Water Content of Rice and Soybean. *IEEE Geoscience and Remote Sensing Letters*, *9*(4), 564–568. https://doi.org/10.1109/LGRS.2011.2174772

Lee, J.-S., & Pottier, E. (2009). *Polarimetric Radar Imaging: From Basics to Applications*. https://doi.org/10.1201/9781420054989

Lindsay, E., Ganerød, A. J., Devoli, G., Reiche, J., Nordal, S., & Frauenfelder, R. (2025). Understanding Landslide Expression in SAR Backscatter Data: Global Study and Disaster Response Application. *Remote Sensing*, *17*(19), 3313. https://doi.org/https://doi.org/10.3390/rs17193313

Liu, B., Chen, Y., Hu, J., Yao, T., Tan, Y., Qin, Z., Wang, C., & Yin, W. (2025). Landslide Identification in the Yuanjiang Basin of Northwestern Hunan, China, Using Multi-Temporal Polarimetric InSAR with Comparison to Single-Polarization Results. *Remote Sensing*, *17*(9), 1525. https://doi.org/https://doi.org/10.3390/rs17091525

Luo, S., Tong, L., Chen, Y., & Tan, L. (2015). Landslides identification based on polarimetric decomposition techniques using Radarsat-2 polarimetric images. *International Journal of Remote Sensing*, *37*, 1–13. https://doi.org/10.1080/01431161.2015.1041620

MapLogs, E. *Enga Elevation Map*. https://elevation.maplogs.com/poi/enga_province_papua_new_guinea.115847.html

Nava, L., Bhuyan, K., Meena, S. R., Monserrat, O., & Catani, F. (2022). Rapid Mapping of Landslides on SAR Data by Attention U-Net. *Remote Sensing*, *14*(6), 1449. https://doi.org/10.3390/rs14061449

Niu, C., Zhang, H., Liu, W., Li, R., & Hu, T. (2021). Using a fully polarimetric SAR to detect landslide in complex surroundings: Case study of 2015 Shenzhen landslide. *Isprs Journal of Photogrammetry and Remote Sensing*, *174*, 56–67. https://doi.org/https://doi.org/10.1016/j.isprsjprs.2021.01.022

Novellino, A., Pennington, C., Leeming, K., Taylor, S., Alvarez, I. G., McAllister, E., Arnhardt, C., & Winson, A. (2024). Mapping landslides from space: A review. *Landslides*, *21*(5), 1041–1052. https://doi.org/10.1007/s10346-024-02215-x

Ohki, M., Abe, T., Tadono, T., & Shimada, M. (2020). Landslide detection in mountainous forest areas using polarimetry and interferometric coherence. *Earth, Planets and Space*, *72*(1), 67. https://doi.org/10.1186/s40623-020-01191-5

Orynbaikyzy, A., Albrecht, F., Yao, W., Motagh, M., Wang, W., Martinis, S., & Plank, S. (2025). Landslide mapping with deep learning: the role of pre- and post-event SAR features and multi-sensor data fusion. *GIScience & Remote Sensing*, *62*(1), 1–25. https://doi.org/10.1080/15481603.2025.2502214

Park, S.-E., & Lee, S.-G. (2019). On the Use of Single-, Dual-, and Quad-Polarimetric SAR Observation for Landslide Detection. *ISPRS International Journal of Geo-Information*, *8*(9), 384. https://doi.org/https://doi.org/10.3390/ijgi8090384

Pepe, A., & Calò, F. (2017). A Review of Interferometric Synthetic Aperture RADAR (InSAR) Multi-Track Approaches for the Retrieval of Earth's Surface Displacements. *Applied Sciences*, *7*(12), 1264. https://doi.org/https://doi.org/10.3390/app7121264

Plank, S., Twele, A., & Martinis, S. (2016). Landslide Mapping in Vegetated Areas Using Change Detection Based on Optical and Polarimetric SAR Data. *Remote Sensing*, *8*(4), 307. https://doi.org/https://doi.org/10.3390/rs8040307

Robbins, J. (2014). Understanding the spatial and temporal occurrence of landslides using satellite and airborne technologies: Papua New Guinea.

Shibayama, T., & Yamaguchi, Y. (2014). A landslide detection based on the change of scattering power components between multi-temporal PolSAR data. 2014 IEEE Geoscience and Remote Sensing Symposium,

Tamm, T., Zalite, K., Voormansik, K., & Talgre, L. (2016). Relating Sentinel-1 interferometric coherence to mowing events on grasslands. *Remote Sensing*, *8*(10), 802. https://doi.org/10.3390/rs8100802

Tolometti, G., Neish, C., Hamilton, C., Osinski, G., Kukko, A., & Voigt, J. (2022). Differentiating Fissure-Fed Lava Flow Types and Facies Using RADAR and LiDAR: An Example From the 2014–2015 Holuhraun Lava Flow-Field. *Journal of Geophysical Research: Solid Earth*, *127*. https://doi.org/10.1029/2021JB023419

UNOSAT. (2024). *Papua New Guinea Landslide – Overview Map (as of 27 May 2024)*. U. N. S. C. (UNOSAT). https://unosat.org/products/3857

Yonezawa, C., Watanabe, M., & Saito, G. (2012). Polarimetric Decomposition Analysis of ALOS PALSAR Observation Data before and after a Landslide Event. *Remote Sensing*, *4*(8), 2314–2328. https://doi.org/https://doi.org/10.3390/rs4082314